# Variance quantification of different additive manufacturing processes for Acoustic Metamaterials

Manuel Bopp[1]
Arn Joerger[2]
Matthias Behrendt [3]
Albert Albers[4]

IPEK – Institute of Product Engineering at Karlsruhe Institute of Technology (KIT)
Kaiserstraße 10
76131 Karlsruhe, Germany

**ABSTRACT**

*Many concepts for acoustic metamaterials rely on additive manufacturing techniques. Depending on the production process and material of choice, different levels of precision and repeatability can be achieved. In addition, different materials have different mechanical properties, many of which are frequency dependent and cannot easily be measured directly. In this contribution the authors have designed different resonator elements, which have been manufactured utilizing Fused Filament Fabrication with ABSplus and PLA, as well as PolyJet Fabrication with VeroWhitePlus.*
*All structures are computed in FEA to obtain the calculated eigenfrequencies and mode shapes, with the respective literature values for each material. Furthermore, the dynamic behavior of multiple instances of each structure is measured utilizing a 3D-Laser-Scanning Vibrometer under shaker excitation, to obtain the actual eigenfrequencies and mode shapes. The results are then analyzed in regards to variance between different print instances, and in regards to accordance between measured and calculated results. Based on previous work and this analysis the parameters of the FEA models are updated to improve the result quality.*

## 1. INTRODUCTION

### 1.1. Acoustic Metamaterial based on resonators

Metamaterials are artificially produced materials with properties that are different from the properties usually observed in naturally occurring materials [1]. The term was originally introduced in the field of electromagnetic wave propagation by Russian physicist Victor Veselago [2], and describes materials that incorporate small periodic structures that result in e.g. negative index of refraction or negative electrical permittivity.

Many of the concepts can be transferred to acoustic wave propagation. Conventional materials such as steel, aluminium or polymers have a well understood dynamic behavior and follow the laws of linear structural dynamics. Acoustic Metamaterials differ from that and display properties like a locally negative dynamic mass or negative dynamic stiffness.

[1] manuel.bopp@kit.edu
[2] arn.joerger@kit.edu
[3] matthias.behrendt@kit.edu
[4] albert.albers@kit.edu

Concepts incorporating small periodic resonator elements have been shown to be extremely efficient in sound absorption, within a narrow frequency band and at a highly sub-wavelength size, e.g. in [3]. Due to the complex geometry of the structures, these concepts usually rely on Additive Manufacturing processes.

### 1.2. Additive Manufacturing

Additive Manufacturing (AM) describes a variety of processes that create objects by directly depositing material, without machining or molding. The object is usually created layer-by-layer and the material is fused by e.g. heat, UV light or chemically. Since the material is directly deposited, there is almost complete geometric freedom, e.g. undercuts or hollow structures can be printed without concern for reachability for tooling etc.

There is a very wide range of materials that can be processed with AM, including many polymers, metals and ceramic materials. Especially in Fused-Filament-Fabrication (FFF) there are also compound materials that have e.g. carbon fibers or other particles in them.

Due to the layer-wise fabrication process there are some inherent limitations in precision, and depending on the specific process the micro structure and therefore the material properties will show certain deviations from the parent material. For FFF this was investigated in detail by the author in [4]. A short summary of these results is given in the next paragraph.

### 1.3. Previous work

In [4] the dynamic behavior of FFF parts made from ABSplus was investigated. As displayed in Figure 1, the filament deposition process results in systematic voids inside the material, that have an influence on the mechanic properties of the resulting parts. These voids depend on many factors such as toolpath parameters, nozzle size, layer height etc. The measurement results showed a high variance in most mechanical parameters, especially in tensile modulus.

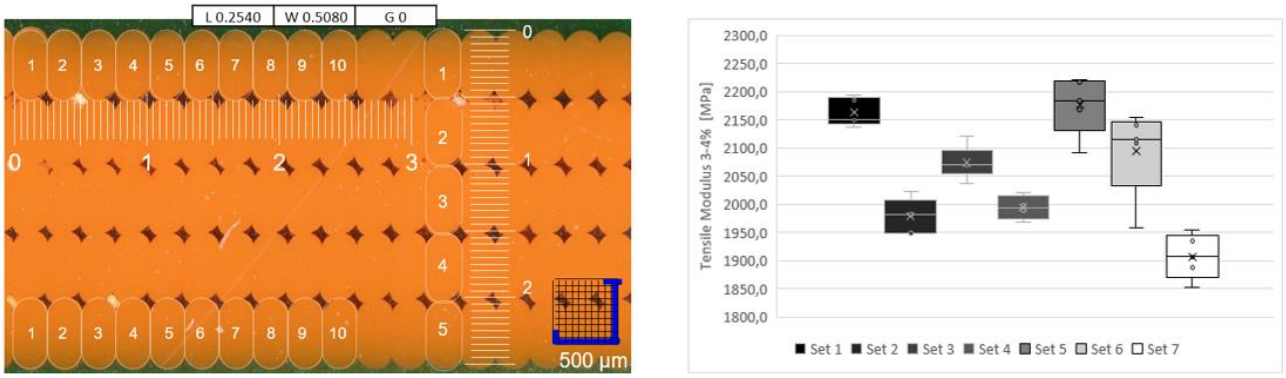


Figure 1: Systematic voids (left) and variance in tensile modulus (right) for parts made from ABSplus [4]

### 1.4. Aim/Scope of work

The working frequency of a metamaterial based on resonator elements is determined by the design of the resonator mass and stiffness. As described, the density and elastic modulus of AM parts can vary strongly depending on the process parameters and also between instances of the same prints.

In this study, a selection of AM processes and materials are investigated regarding their suitability for producing acoustic metamaterials. Resonator elements with different dimensions are designed, fabricated and measured with a 3D Laser-Scanning-Vibrometer. The measured data is analyzed regarding resonance frequency, variance, damping and accordance with FEA results.

## 2. RESONATOR DESIGN

### 2.1. Resonator Design 1

The first design is a full array of resonator elements directly printed on a carrier plate. It consists of five rows with five identical resonators in each row, as depicted in Figure 2.

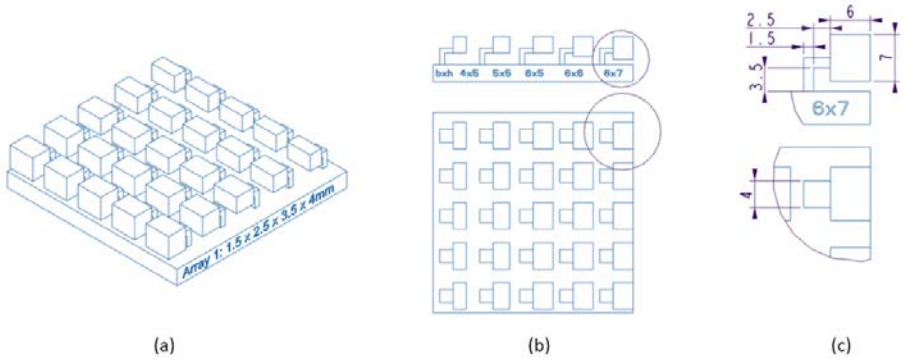


Figure 2: Multiple resonators on a carrier plate (here: Array 1)

Each row has a different mass element (see Table 1) and overall there are three arrays with different dimensions of the spring element (the "arm" of the resonator element) (comp. Figure 2c):

- Array 1 Arm Dimensions: 1.5 x 2.5 x 3.5 x 4 mm
- Array 2 Arm Dimensions: 1.0 x 2.5 x 3.5 x 4 mm
- Array 3 Arm Dimensions: 1.5 x 2.5 x 3.5 x 3 mm

Table 2: Geometric properties of the mass elements, nominal and average actual mass for design 1

| Row No. | Depth [mm] | Width [mm] | Height [mm] | $m_{Nominal}$ ABSplus [g] | $m_{Average}$ ABSplus [g] | $m_{Nominal}$ VeroWhite [g] | $m_{Averag}$ VeroWhite [g] |
|---|---|---|---|---|---|---|---|
| 1 | 8 | 4 | 5 | 0,17 | 0,12 | 0,19 | 0,18 |
| 2 | 8 | 5 | 5 | 0,21 | 0,19 | 0,23 | 0,21 |
| 3 | 8 | 6 | 5 | 0,25 | 0,22 | 0,28 | 0,27 |
| 4 | 8 | 6 | 6 | 0,30 | 0,26 | 0,34 | 0,32 |
| 5 | 8 | 6 | 7 | 0,35 | 0,32 | 0,39 | 0,38 |

The design is very practical in terms of handling and measurement setup, as all top surfaces are in the same plane and all 25 resonators can easily be measured in one session. However, there was a noticeable influence on the measurement results caused by the modal behavior of the carrier plate itself. Another problem was that with certain additive manufacturing processes the support material could not be removed properly or without breaking off resonators, which also had some influence on the measured results. For this reason, a second design was developed.

### 2.2. Resonator Design 2

Due to the problems occurring with the first design another concept for the resonators was designed. The design can be seen in Figure 3. It consists of a single resonator element on a support plate. The geometry of the arm is simplified and a fillet is introduced on the bottom to reduce stress and prevent breaking.

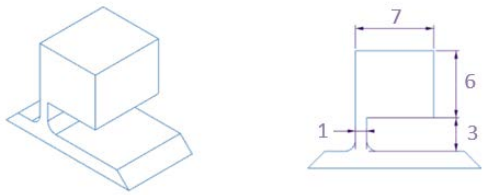


Figure 3: Single resonator design (here: ID1500)

In this design the number of parameters is reduced. The strength of the arm is kept at 1 mm, the depth of the whole element is fixed at 8 mm and the width at 7 mm. Only the length of the arm and the height of the mass element are varied as follows:

Table 3: Identifier and geometric parameters for design 2

| Element ID | Depth [mm] | Width [mm] | Height [mm] | Arm Length [mm] |
|---|---|---|---|---|
| 1000 | 8 | 7 | 4 | 2 |
| 1100 | 8 | 7 | 5 | 2 |
| 1200 | 8 | 7 | 6 | 2 |
| 1300 | 8 | 7 | 4 | 3 |
| 1400 | 8 | 7 | 5 | 3 |
| 1500 | 8 | 7 | 6 | 3 |

## 3. ADDITIVE MANUFACTURING PROCESS AND MATERIALS

The resonator elements are fabricated with different additive manufacturing (AM) technologies and materials, which are briefly introduced in this section.

### 3.1. Fused Filament Fabrication

FFF is one of the most common AM processes, for a number of reasons. The overall handling of the process and filament is relatively easy, the printers and materials are affordable and there is a very wide variety of materials to choose from.

In FFF, the material is fed into the printer as a continuous filament string, heated until its melting point and then deposited onto a print bed through a nozzle. Usually the printing head with the nozzle is moving in x- and y- direction, printing one layer of the model at a time, and then either the printhead is moved up or the print bed is lowered by one layer height. Depending on the printer, the support material for overhanging structures can be either the same material or a second material that is e.g. soluble, which makes the removal of support structure a lot easier. In this study two different FFF printers are utilized:

*Stratasys Dimension Elite* (s. Figure 4 left) is an industry level FFF printer from 2014 with fully enclosed, heated building environment. The model material used is *ABSplus* from *Stratasys* and support material is a second material that is soluble in sodium hydroxide

*Creality Ender 3 v2* is a consumer level FFF printer from 2020 with heated print bed. As model material two different PLAs are used (*extrudr PLA nx2 black* and *Amazon Basics PLA black*)

Figure 4: *Stratasys Dimension Elite* (left) [5], *Creality Ender 3 v2* (middle) [6] and *Stratasys Objet260 Connex1* (right) [7]

### 3.2. PolyJet Modeling

PolyJet Modeling is an AM process based on liquid resin droplets that are hardened by UV light. Its working principle is similar to that of a conventional inkjet printer. Multiple materials can be loaded simultaneously in a cartridge as liquid resin, and are then dispensed at the desired position in form of very small droplets, and subsequently hardened by UV light.

The printer used in this study is a *Stratasys Objet260 Connex1* with the material *VeroWhite.*

## 4. EXPERIMENTAL SETUP

The resonators are measured using a 3D Laser-Scanning-Vibrometer (LSV) and shaker excitation. As excitation signal a pseudo random signal is used. The specimen is mounted to a force sensor that is connected to the shaker over a stinger, as shown for design 2 in Figure 5. Except for the Vero specimens, all the surfaces were prepared with white paint marker to improve reflectiveness for the LSV.

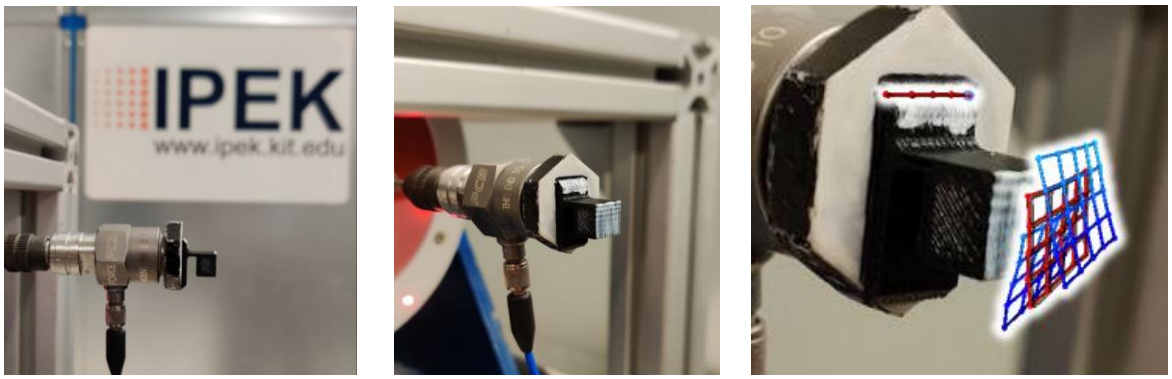


Figure 5: Single resonator mounted on the force sensor and animated measurement points (right)

The measurement points are defined as shown in Figure 5 on the right-hand side. There are five points on the top of the base pate as reference, to detect effects that result from the modal behavior of the stinger-sensor-assembly. On the mass element there are 25 measurement points in a rectangular shape. For the calculation of the following Frequency Response Functions (FRFs) the reference points on the base plate have been deactivated.

## 5. MEASUREMENT RESULTS

### 5.1. Resonator Design 1

Design 1 was first printed and measured in ABS and VeroWhite. Due to the problematic behavior of the design no specimens were printed in PLA. For the same reason the FRFs are not discussed here but only the extracted eigenfrequencies are shown.

Each array has five rows with different mass elements with dimensions between 4 mm and 7 mm (comp. Figure 2). For ABS two instances of each array were printed, and the particular instances of e.g. array 1 are named 11 and 12 etc., as shown in Figure 6 and separated left and right in each diagram. For VeroWhite only two instances of array 1 were printed, since it was almost impossible to remove the support structure without breaking off resonators. For this reason, only one instance of VeroWhite has been measured.

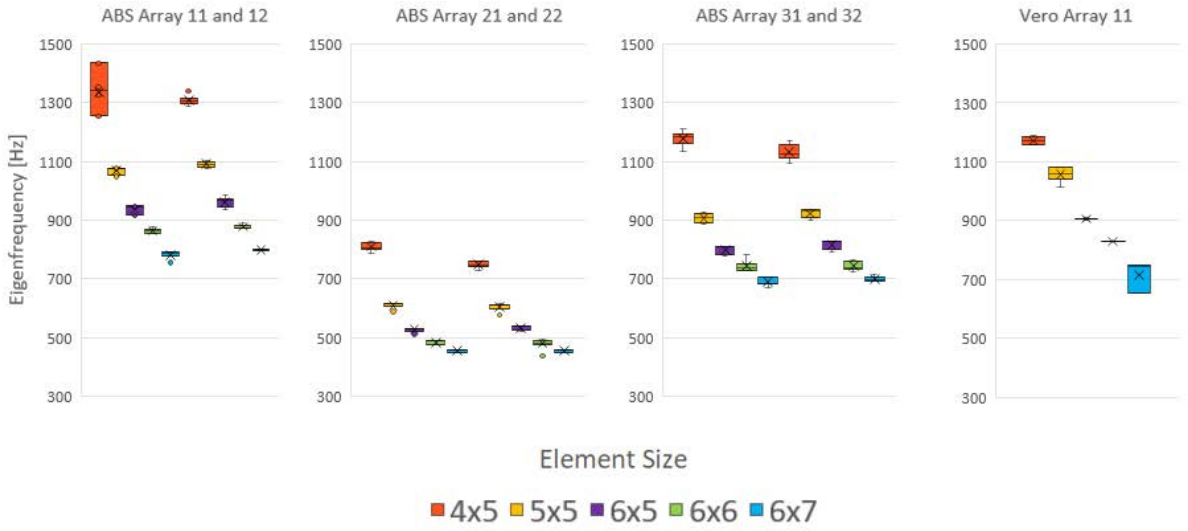


Figure 6: Eigenfrequencies for ABS and Vero arrays, colors indicate the size of the mass element

### 5.2. Resonator Design 2

For design 2 there are six different geometries labeled 1000-1500. Each geometry is printed in 4 different materials labeled *ABS, PLAa, PLAx,* and *Vero*. In this section the FRFs for each material and printing process are discussed. In Appendix A the curves are also displayed sorted by geometry.

**ABSplus on Stratasys Printer**

The FRFs for ABS show relatively high variance, especially in the higher frequency range. The two blue lines peaking at 3000 Hz are two separate measurements of the same specimen. This shows that there is some variance in the measurement setup and the mounting of the specimen too.

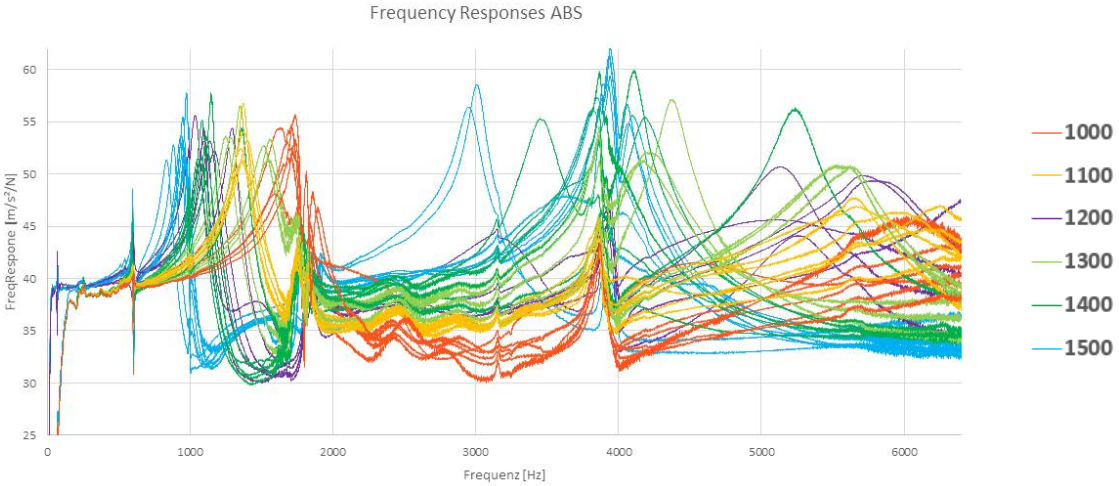


Figure 7: FRFs of all ABS specimen grouped by geometry ID

Some of the peaks are present at the same frequencies over all materials and geometries, especially the large peak at 3900 Hz. These effects can be linked to the modal behavior of the stinger-sensor assembly itself and will not be analyzed in detail in this contribution. Since these effects are interfering with some of the higher modes, only the first eigenfrequency of each sample is extracted and summarized for all materials in Figure 13. The individual groups in ABS show a variance of approx. 150 Hz, a standard deviation has not been calculated due to the small sample size per group.

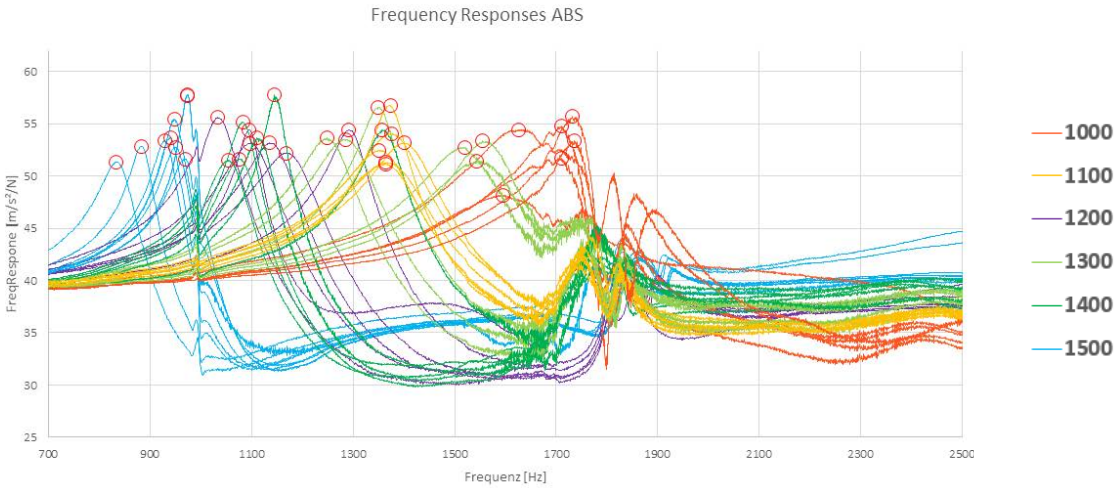


Figure 8: Detailed FRFs of the first resonance of ABS specimen with marked peak values

**PLA on consumer FFF printer**

The FRFs for PLAa show less variance, except for ID1000. Since PLA has a higher damping than ABS the amplitudes are noticeably lower here, especially in the higher frequency range. Compared to the first PLA, the PLAx shows much higher variance. For the prints with the PLAx the printing temperature was increased from 195°C to 200°C in order to reduce smearing.

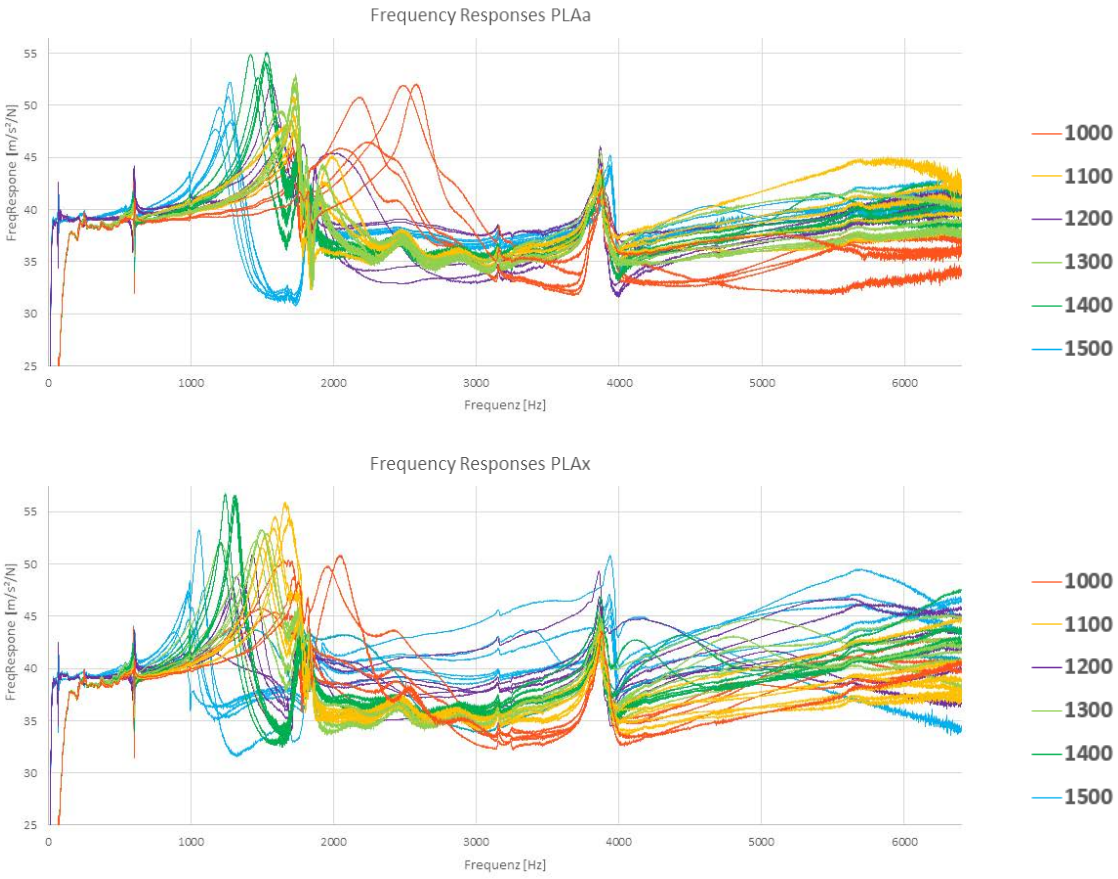


Figure 9: FRFs of all PLA specimen grouped by geometry ID

When compared in detail, there is a noticeable difference in the first eigenfrequencies between the two PLA materials. It is suspected that the change in print temperature is responsible, since it has a great influence on the bonding between layers and the smearing of the material. Higher degree of smearing could potentially lead to higher amount of cross-connections, which can explain increased stiffness in the PLAa specimen.

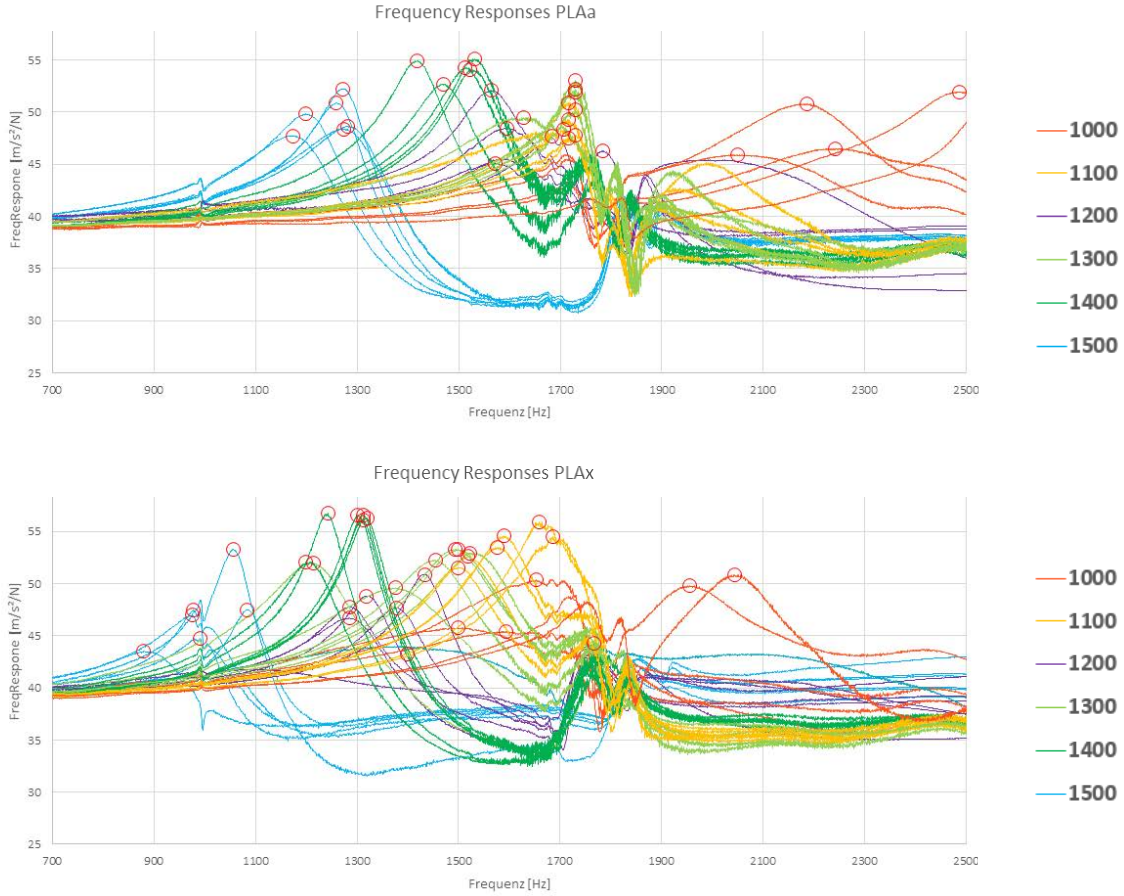


Figure 10: Detailed FRFs of the first resonance of all PLA specimen with marked peak values

**VeroWhite on PolyJet printer**

The specimen printed with MultiJet Modeling had the overall lowest variance and showed similar behavior over the whole spectrum. The material behaves similar to PLA and shows relatively high damping, especially at higher frequencies.

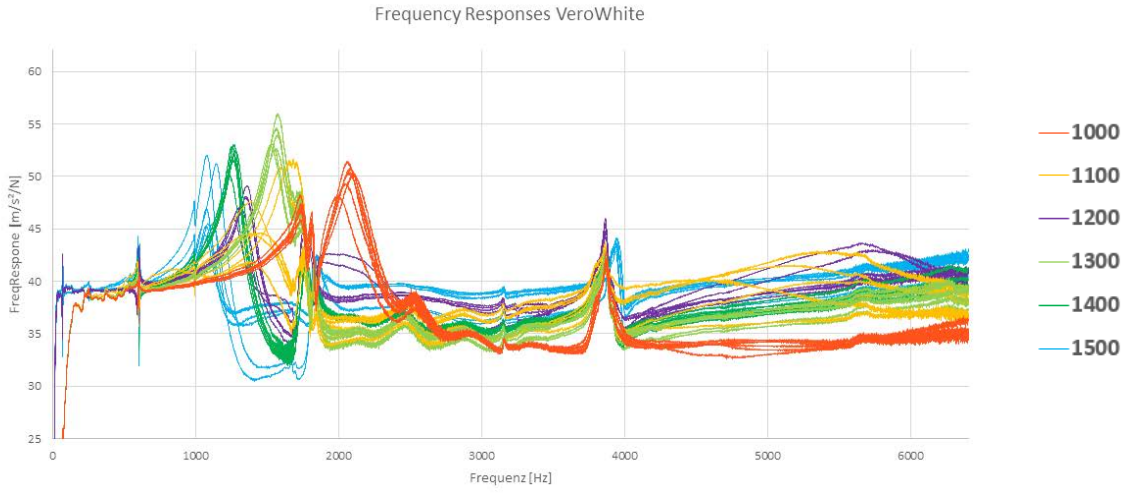


Figure 11: FRFs of all Vero specimen grouped by geometry ID

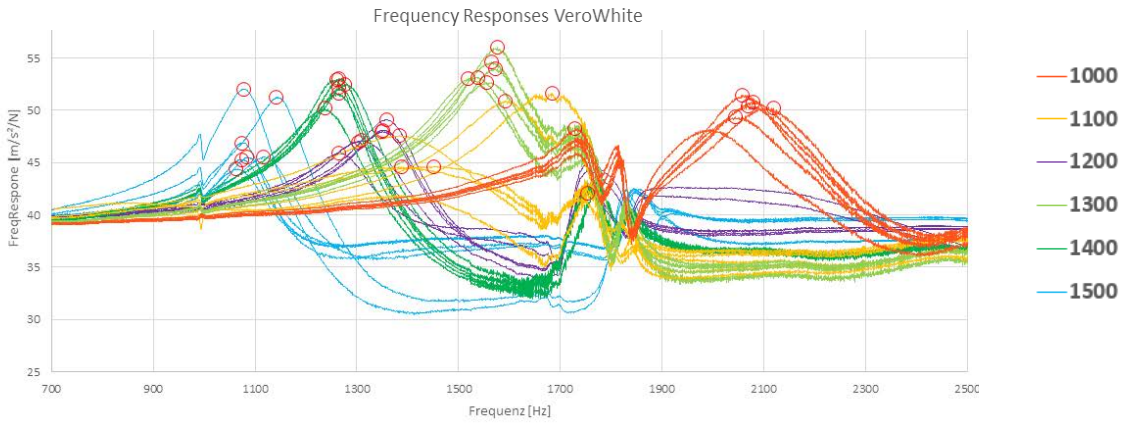


Figure 12: Detailed FRFs of the first resonance of all Vero specimen with marked peak values

### 5.3. Summary

The eigenfrequencies of the resonators behave overall as expected. With larger mass and lower stiffness, the frequencies move down (ID1000 - 1200), from ID1200 to ID1300 there is a step upwards since the mass is set back to the smallest (same as in ID1000), while the stiffness of the arm is decreased for ID1300, 1400 and 1500. The overall variance for the first mode is relatively high and averages around 10% for all filament-based processes. The frequent occurrence of outliers and overall poor reproducibility make a precise design of metamaterials with the measured processes difficult.

The measurements were also influenced by the modal behavior of the sensor assembly. Figure 14 shows the FRFs of some of the measured reference points on the base plate of the specimen. The modal behavior of the assembly can clearly be seen at 600 Hz, 1000 Hz, 1700 Hz and 3900 Hz.

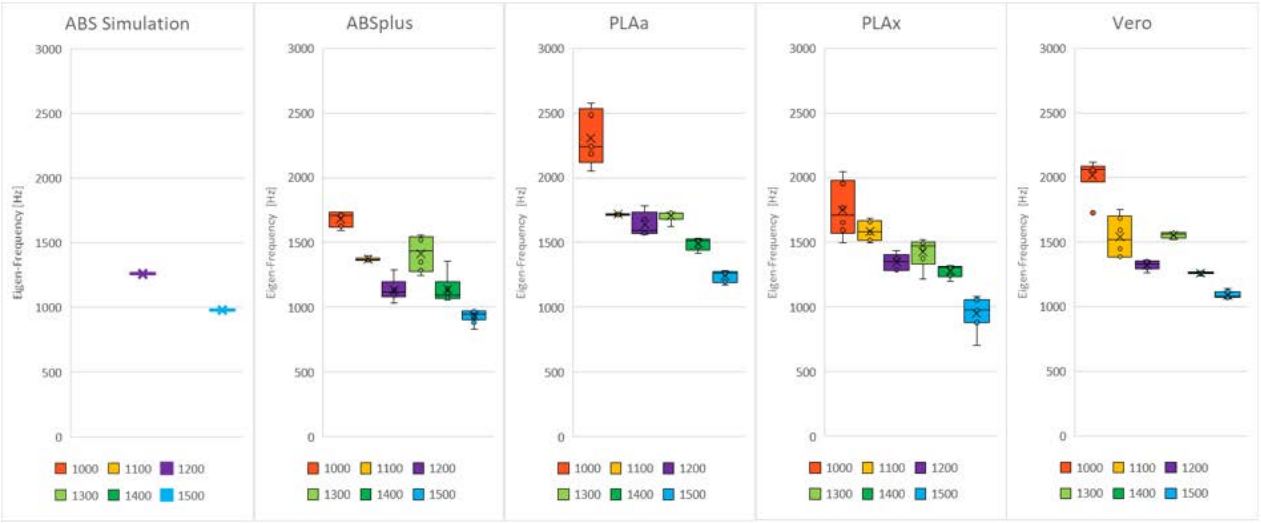


Figure 13: Extracted first eigenfrequencies of all specimen from design 2 and simulation result for ABS ID1200 and ID1500 (left)

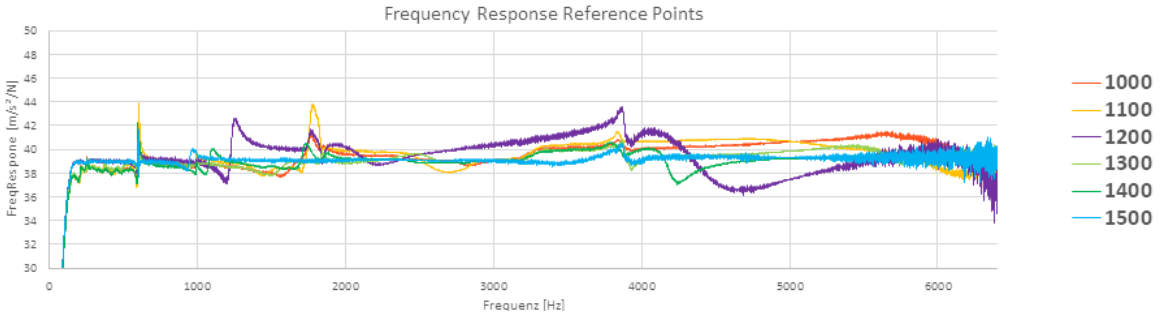


Figure 14: FRFs of reference points show the modal behavior of the sensor assembly

## 6. FEA DESIGN

Two selected designs (ID1200 and ID1500) were modeled and computed in the FE-Software *Dassault Abaqus 2019*. The aim of the computation was to analyze the deviations between the simulation and the physical experiments. Both models consist of the lower base plate and the upper geometry. The base plate is fixed. The analysis considers a frequency range between 0 and 10 kHz. The material is modeled isotropic with the parameters shown in Table 4. As shown in [4], the Youngs Modulus of ABS is frequency dependent and typically increases about 150 MPa per decade (see Appendix B). The frequency dependence is not implemented in the simulation. The FE simulations comprise eight models with varying element types (hexahedral and tetrahedral) and two element sizes (0.25 mm and 0.1 mm).

Table 4: Material properties for ABSplus used for the FEA

| Young's Modulus | Poisson Ratio | Density |
|---|---|---|
| 2100 MPa | 0.29 | 1.04 g/cm³ |

### 6.1. FEA Results

The results are displayed in Table 5. The values show that tetrahedral meshes tend to higher frequencies in comparison to hexahedral. But with hexahedral elements, the frequencies decrease with increasing element size, whereas with tetrahedral elements the frequencies increase. However, the variance in the simulation results is smaller than the variance in the physical measurements. Because the tetrahedral models with element size 0.1 represent the geometry best and the computation time is affordable for this research, these setting are be used for the further simulations.

Table 5: Results of the mesh study and comparison to measured frequencies

| Model | Mode 1 [Hz] | Mode 2 [Hz] | Mode 3 [Hz] |
|---|---|---|---|
| **ID1200 Measured** | **1137** | **4276** | **6331** |
| ID1200 Hex 0.1 | 1255 | 4187 | 9149 |
| ID1200 Hex 0.25 | 1230 | 4180 | 9138 |
| ID1200 Tet 0.1 | 1261 | 4197 | 9151 |
| ID1200 Tet 0.25 | 1264 | 4212 | 9153 |
| **ID15 Measured** | **952** | **1772** | **4982** |
| ID1500 Hex 0.1 | 988 | 2965 | 7265 |
| ID1500 Hex 0.25 | 960 | 2940 | 7218 |
| ID1500 Tet 0.1 | 986 | 2974 | 7291 |
| ID1500 Tet 0.25 | 988 | 2983 | 7325 |

The computed mode shapes fit well for all modes for both IDs. In Figure 16 and Figure 17 the measurement points are displayed as introduced in Figure *5*. Both maximum displacement positions are shown to visualize the mode shape. Regarding the computed values, the mode 1 simulation values fit well for both models with the physical results. This is also the main mode of interest for the metamaterial. The computation mode 2 for ID1200 has a deviation of less than 5 %, the computed values for the other modes however differ strongly. As depicted in Figure 16 and 15, the reference points on the base plate show movement too for some mode shapes. This suggests that there is an underlying mode of the stinger-sensor-assembly, that interferes with the measurements.

Since the shaker can only excite up to 6.4 kHz, the responses at higher frequencies could not be examined.

**Element 12**

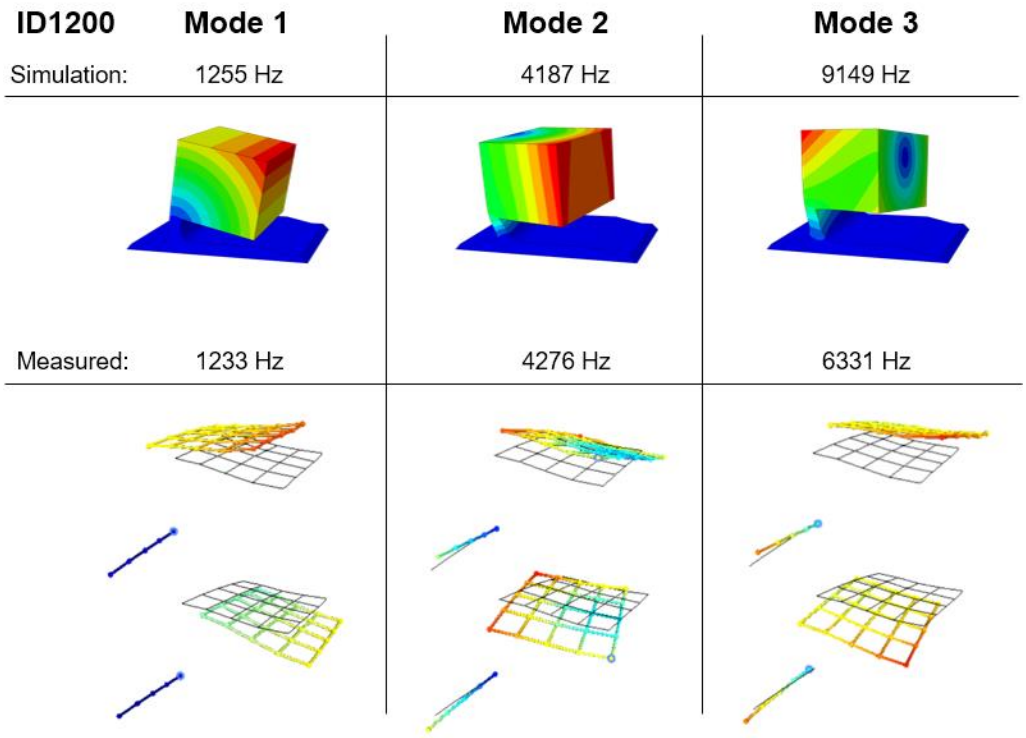


Figure 16: First three modes for the ID1200 Element, simulation and measurement

**Element 15**

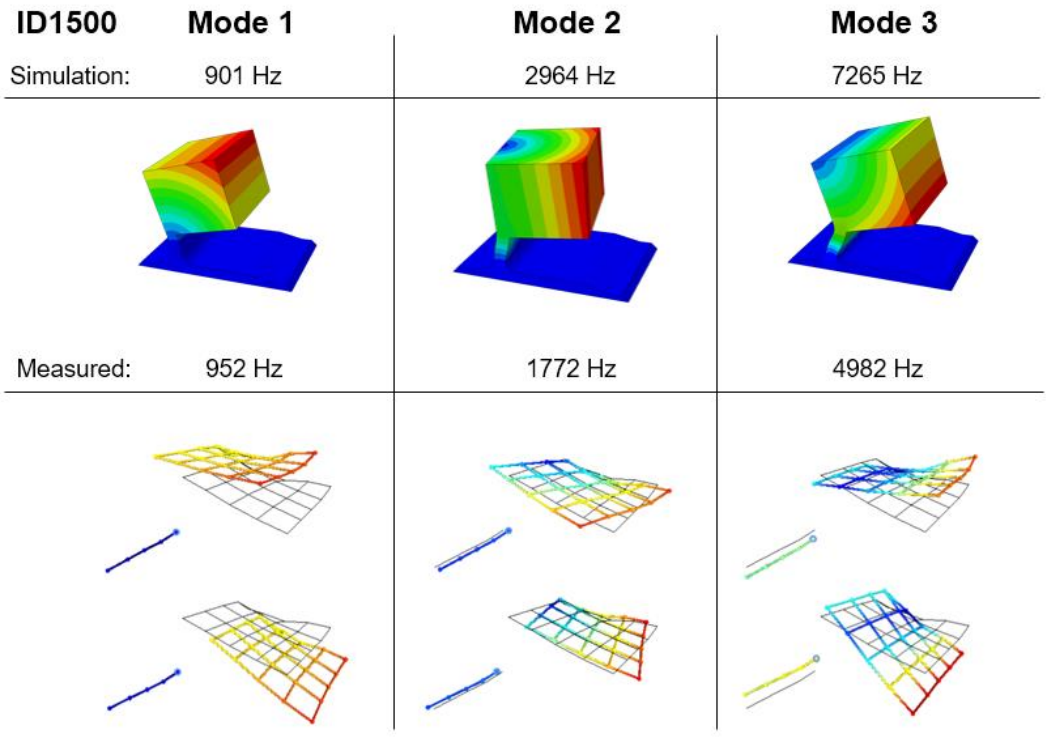


Figure 17: First three modes for the ID1500 Element, simulation and measurement

The deviation in mode frequencies resulting from the mesh parameters is small in contrast to the deviation in the physical measurements. This shows that the model input data such as the material properties or the 3D-printed geometry is important for accurate simulation, but process control for the actual fabrication processes needs to be improved in order to get more reproducible specimen.

## 7. CONCLUSIONS

Different conclusions can be drawn from the presented data. Regarding the material, ABS with its low internal damping showed the highest peaks in the FRFs, which should result in the highest absorption of oscillation energy in an actual use case. All other materials showed significantly lower amplitudes, especially in the higher frequency range.

Regarding the fabrication processes, the PolyJet parts showed the highest precision and reproducibility of all investigated processes. The filament-based processes had frequent outliers and generally low reproducibility, independent from the printer and material.

The comparison with the FE models showed a good general accordance of the found mode shapes, and of some eigenfrequencies. Especially the eigenfrequencies of the first mode could be met in the FEA relatively precisely. Eigenfrequencies of higher modes did not show good accordance and will be investigated in further research.

The measured data will also be analyzed in further detail. Due to the very small mass of the specimen, the modal behavior of the shaker-stinger-sensor assembly had a high influence on the measurements. It is suspected that when specimen have eigenfrequencies in the same range as the overall assembly, the modal behavior of the specimen is concealed by the much higher amplitudes of the assembly, especially since the excitation force is only measured in y-direction, but many of the higher mode shapes have high proportions of x- and z- movement.

## 8. REFERENCES


[1] Kshetrimayum, R.S., "A brief intro to metamaterials," *IEEE Potentials* 23(5):44–46, 2005, doi:10.1109/MP.2005.1368916.

[2] Veselago, V.G., "THE ELECTRODYNAMICS OF SUBSTANCES WITH SIMULTANEOUSLY NEGATIVE VALUES OF ε AND μ," *Sov. Phys. Usp.* 10(4):509–514, 1968, doi:10.1070/PU1968v010n04ABEH003699.

[3] Claeys, C., Deckers, E., Pluymers, B., and Desmet, W., "A lightweight vibro-acoustic metamaterial demonstrator: Numerical and experimental investigation," *Mechanical Systems and Signal Processing* 70-71:853–880, 2016, doi:10.1016/j.ymssp.2015.08.029.

[4] Bopp, M. and Behrendt, M., "Dynamic Mechanical Analysis of FFF Printed Parts in ABSplus: INTERNOISE Proceedings 2020," *INTERNOISE 2020*, Seoul.

[5] Stratasys, "Dimension Elite User Guide," https://support.stratasys.com/sitecore/api/downloadazurefile?id=59005a10-cd4d-4a74-ac84-da83ec5e8ce9, March 18, 2021.

[6] Creality 3D EU, "Creality 3D Ender 3 v2," https://www.creality3dshop.eu/collections/ender-series-3d-printer/products/creality3d-upgraded-ender-3-v2-3d-printer, March 18, 2021

[7] Stratasys, "Objet260 Connex1 User Guide," https://support.stratasys.com/sitecore/api/downloadazurefile?id=e2bb8fba-c3ef-4e77-8238-07db8d4d82b6, March 18, 2021.

# APPENDIX A

## Frequency Response Functions sorted by geometry

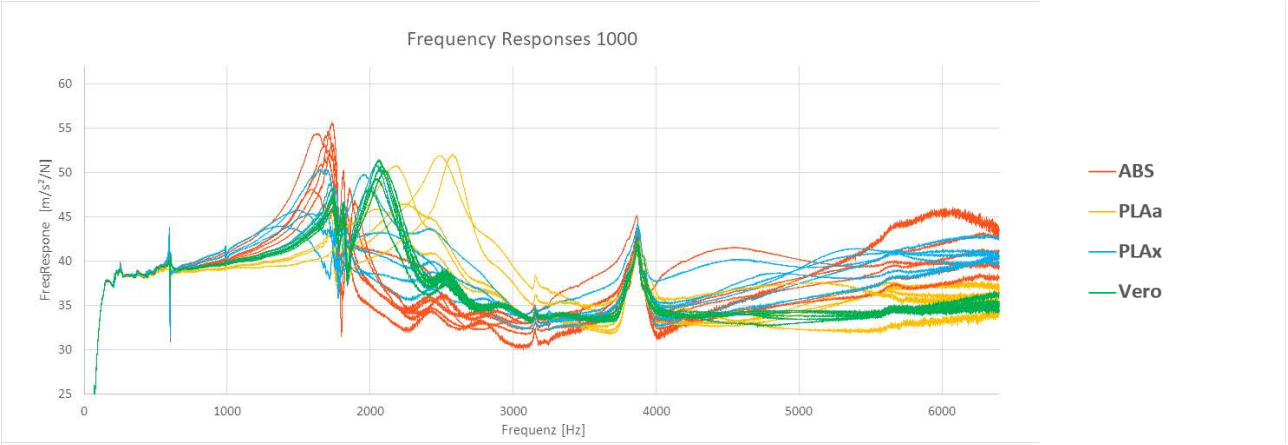


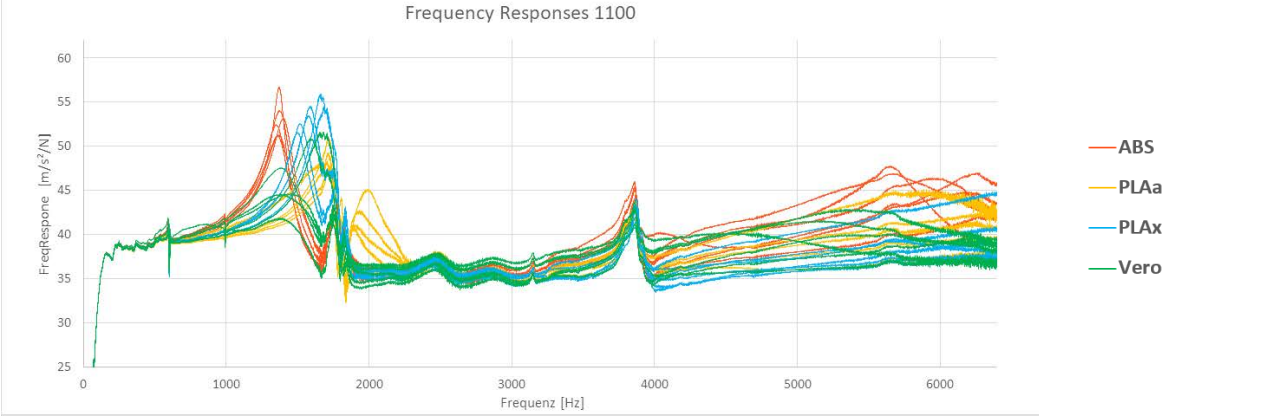


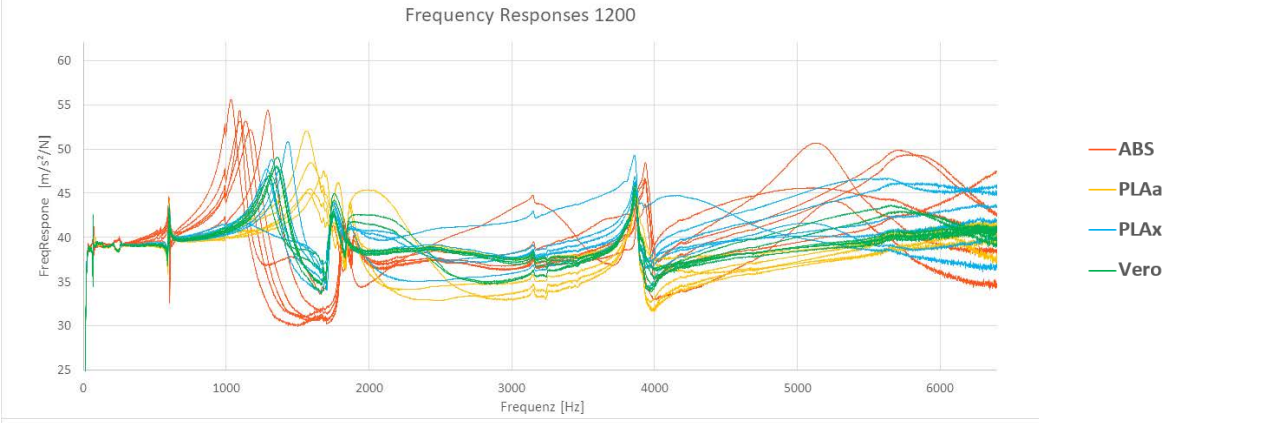


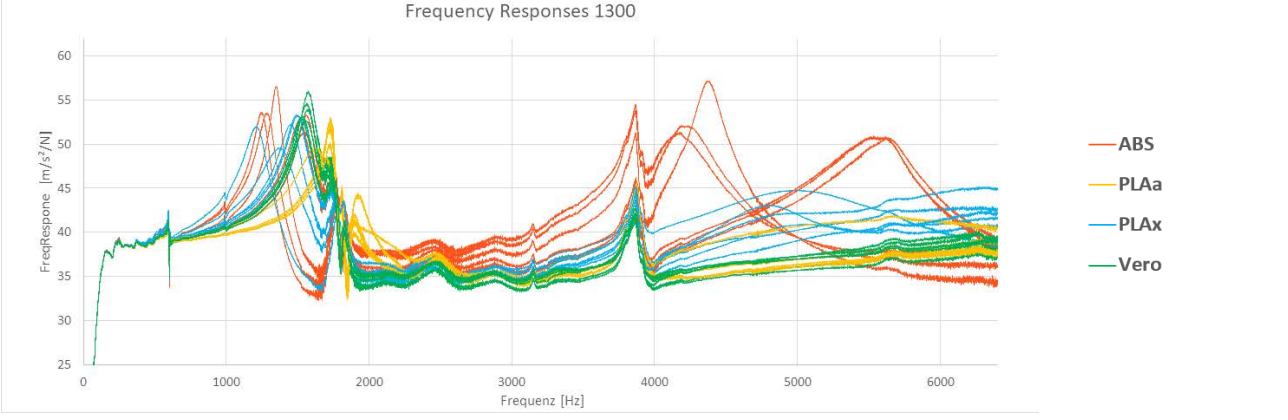

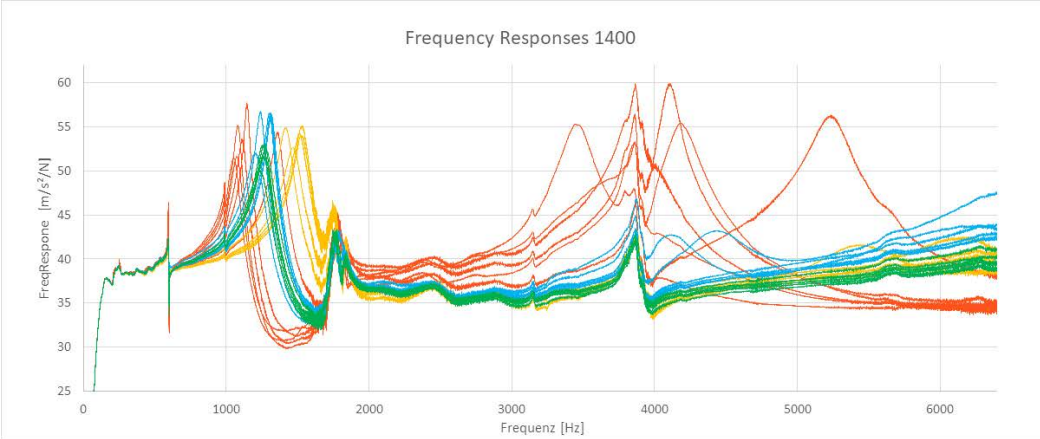


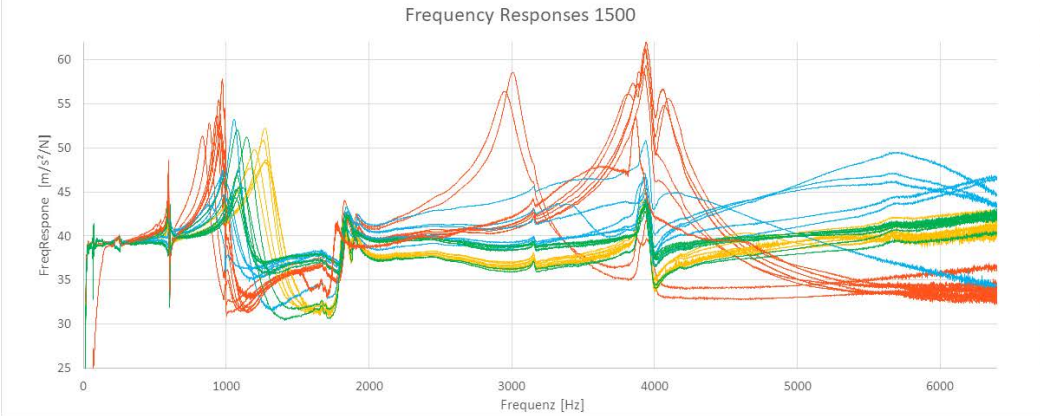


## Frequency Response Functions sorted by geometry, detailed view of 1st mode

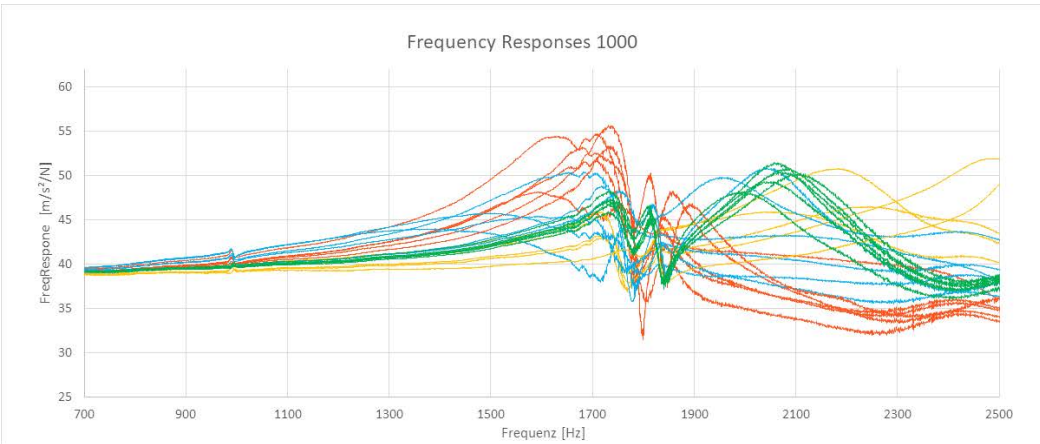


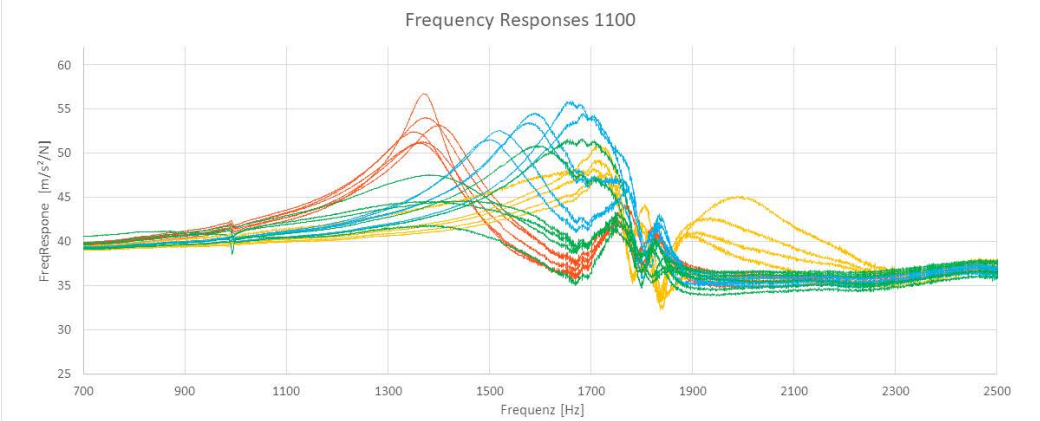

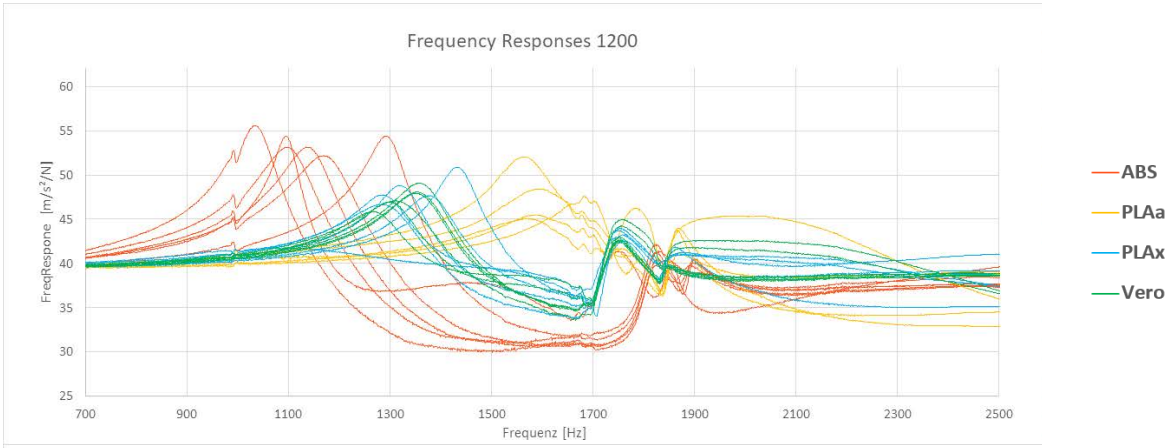
Frequency Responses 1200
FreqRespone [m/s²/N]
Frequenz [Hz]
ABS
PLAa
PLAx
Vero

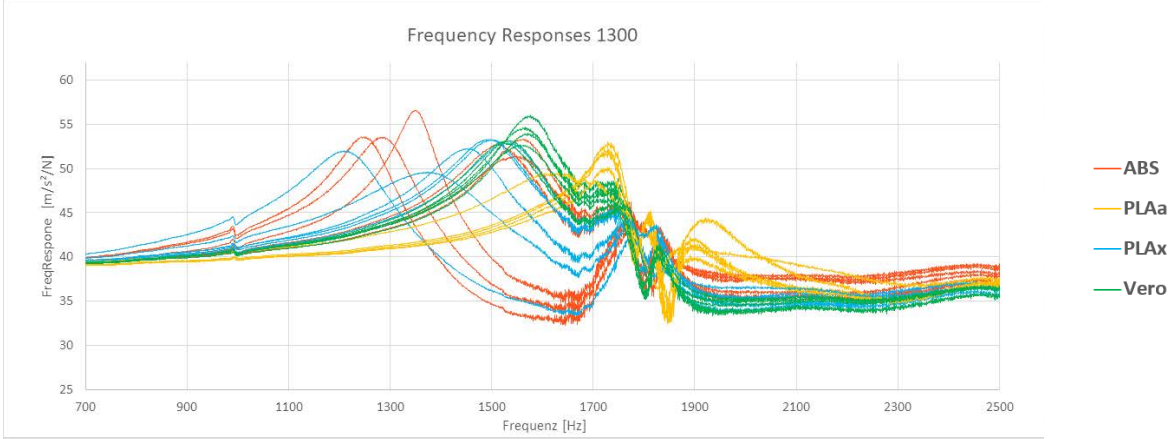
Frequency Responses 1300
FreqRespone [m/s²/N]
Frequenz [Hz]
ABS
PLAa
PLAx
Vero

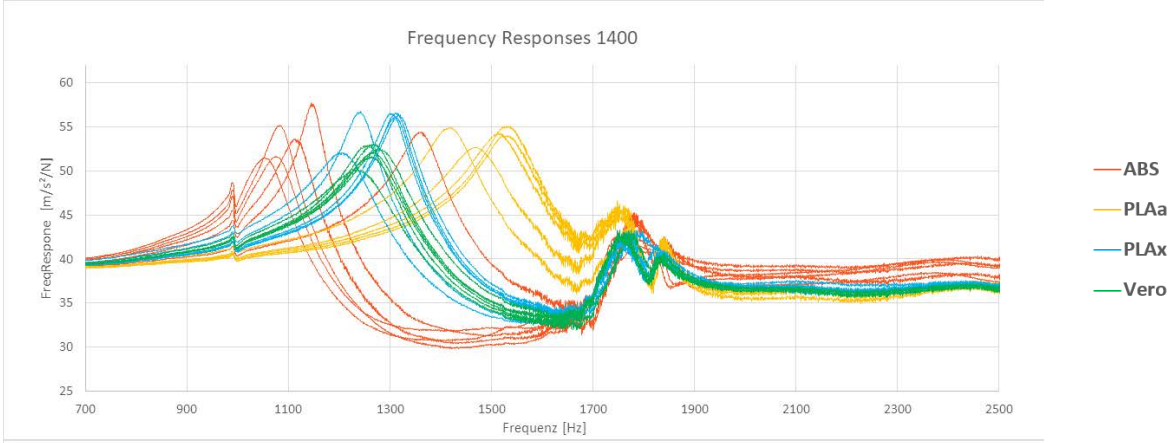
Frequency Responses 1400
FreqRespone [m/s²/N]
Frequenz [Hz]
ABS
PLAa
PLAx
Vero

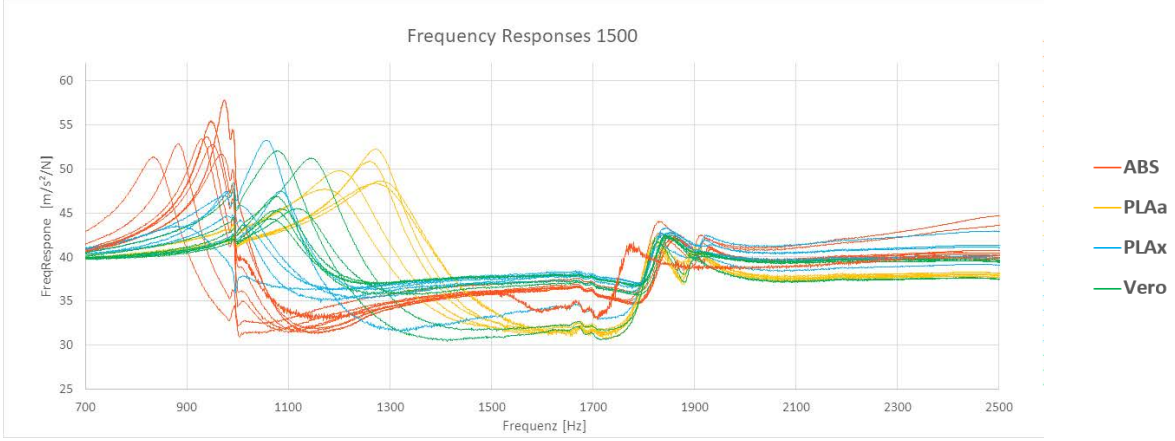
Frequency Responses 1500
FreqRespone [m/s²/N]
Frequenz [Hz]
ABS
PLAa
PLAx
Vero

## APPENDIX B

## Master curves of storage modulus and loss factor for ABS [4]